Variations in Central Asian dust activity and potential driving mechanisms over the past 80 kyr

Article *in* Gondwana Research · May 2025

DOI: 10.1016/j.gr.2025.03.020

10 authors, including:

Haoru Wei
Institute of Earth Environment, Chinese Academy of Sciences
5 PUBLICATIONS **11** CITATIONS
SEE PROFILE

Yougui Song
Institute of Earth Environment, Chinese Academy of Sciences
220 PUBLICATIONS **6,511** CITATIONS
SEE PROFILE

Mingyu Zhang
6 PUBLICATIONS **15** CITATIONS
SEE PROFILE

Hamid Gholami
University of Hormozgan
184 PUBLICATIONS **1,891** CITATIONS
SEE PROFILE

Gondwana Research 144 (2025) 77–86

Contents lists available at ScienceDirect

Gondwana Research

journal homepage: www.elsevier.com/locate/gr

Variations in Central Asian dust activity and potential driving mechanisms over the past 80 kyr

Haoru Wei [a,b], Yougui Song [a,*], Yanping Wang [a,b], Mingyu Zhang [a,c], Hamid Gholami [d], Shugang Kang [a], Yue Li [a], Shukhrat Shukurov [e], Nosir Shukurov [e], Rustam Orozbaev [f]

[a] State Key Laboratory of Loess Science, Institute of Earth Environment, Chinese Academy of Sciences, Xi'an 710061, China
[b] University of Chinese Academy of Sciences, Beijing 100049, China
[c] Xi'an Institute for Innovative Earth Environment Research, Xi'an 710061, China
[d] Department of Natural Resources Engineering, University of Hormozgan, Bandar Abbas 7916193145, Iran
[e] Institute of Geology and Geophysics, University of Geological Sciences, Ministry of Mining Industry and Geology of the Republic of Uzbekistan, Tashkent 100164, Uzbekistan
[f] Institute of Geology, National Academy of Sciences of Kyrgyz Republic, Bishkek 720040, Kyrgyzstan

ARTICLE INFO

Handling Editor: Mark Allen

Keywords:
Central Asian loess
Dust accumulation rates
Dust activity
Mean grain size
Westerlies

ABSTRACT

Loess plays a vital role in unraveling the dynamics of dust activity and its implications for climate change. In recent years, the study of dust activity in Central Asian loess has gradually enriched. However, there is a notable gap in comprehensive studies addressing on the long-term changes in dust accumulation rates (DAR) and mean grain size (MGS) in Central Asian loess, and the primary factors influencing aeolian loess deposition remain a subject of debate. In this study, we address this gap by synthesizing DARs data from 42 loess profiles in Central Asia with radiometric dating including OSL and radiocarbon, normalizing and overlapping the DAR and MGS data using the Z-score method. The results show that the DAR of the loess in Central Asian subregions I and II increased from MIS5 to MIS3, reached the highest in MIS3, decreased from MIS3 to mid-Holocene, and increased after mid-Holocene. The variation of DAR in subregion III has been more consistent with the other two subregions since Holocene. The DAR and MGS trends in Central Asian loess are in sync, effectively indicating the Central Asian dust activity since 80 thousand years (kyr) ago. The dust activity in Central Asia is mainly dominated by intense of westerlies which is controlled by precession and obliquity leading to changes in water vapor and wind power. Siberian High and local glacier activities also affect Central Asian dust activity. This study reveals dust activity and driving mechanisms in Central Asia over the past 80 kyr.

1. Introduction

Central Asia, located in the heart of the Eurasian continent, is a vast mid-latitude region stretching from the Caspian Sea in the west to northwest China in the east, and loess is widely distributed in Central Asia (Dodonov, 1991; Song et al., 2021). Loess in Central Asia serves as a valuable sedimentary archive, offering insights into past climatic and environmental changes. Consequently, studies on Central Asian loess have experienced a steady surge in recent years (Machalett et al., 2008; Song et al., 2015; Fitzsimmons et al., 2018; Yang et al., 2020a; Y. Li et al., 2021b; G. Li et al., 2024; Zan et al., 2023).

The study of dust accumulation rates (DAR) in Central Asia helps understand the changes of dust activities over long time scales (Li et al., 2019b, 2021b; Yang et al., 2020b). Simultaneously, variations in dust accumulation rates over a specific period can serve as indicators of conditions in the dust source area, including factors such as wind speed, transport processes, and the deposition of dust through dry or wet settings (Kohfeld and Harrison, 2001; Maher et al., 2010; Mayaud et al., 2016; Ujvari et al., 2017). There are abundant studies on DAR of Central Asian loess in recent years (Li et al., 2016a; Yang et al., 2021; Li et al., 2021b). However, systematic investigations into DAR in Central Asian loess are relatively scarce. Kang et al. (2022) meticulously reconstructed the changes in mass accumulation rates (MARs) within the upper Ili Basin since 30 kyr; while Dave et al. (2023) comprehensively examined the spatial and temporal differences in MARs of different profiles dating back to 60 kyr in the lower Ili Basin in southeast Kazakhstan.

* Corresponding author.
E-mail address: syg@ieecas.cn (Y. Song).

https://doi.org/10.1016/j.gr.2025.03.020
Received 29 October 2024; Received in revised form 10 March 2025; Accepted 28 March 2025
Available online 5 May 2025

Nevertheless, prior systematic studies on Holocene DAR in Central Asian loess predominantly concentrated on the Ili Basin. This highlights a notable gap in the research landscape, with a lack of synthesized investigations on a larger geographical and longer temporal scale across the broader region of Central Asia.

Furthermore, grain size, as a commonly used paleoclimatic indicator in Central Asian loess research, is abundant studies on grain size in Central Asia; it can reflect dust activity in Central Asia on different time scales (Jia et al., 2018; Li et al., 2019b; Cheng et al., 2020; G. Li et al., 2024; Y. Li et al., 2024; Shu et al., 2025). However, there are relatively few comprehensive studies on grain size in Central Asian loess, and the time scale are relatively short (Kang et al., 2022; Fan et al., 2023a; Li et al., 2024). Kang et al. (2022) synthesized the mean grain size of the ZS, TLD, and XEB sections in the Ili Basin to discuss the changes in dust activity of the Ili Basin since 30 kyr ago; Li et al. (2024) compared the > 63 μm grain size fraction of multiple sections in Central Asia with other indicators to discuss Central Asian dust activity since the Holocene; Fan et al. (2023a) selected multiple Central Asian loess sections from different latitudes, capturing the westerly signals in grain size to discuss the migration of the westerly axis during the Heinrich 2 event period. Therefore, it is still necessary to integrate grain size indicators of Central Asian loess on a longer time scale, combined with DAR records to discuss dust activity in Central Asia.

The controlling factors of Central Asian dust activity are also controversial. Some studies believe that the dust activity recorded in the Fergana Valley and Tajik basins loess is changed by atmospheric circulation patterns which are controlled by the global ice volume since the last glaciation (Tian et al., 2021; Li et al., 2021b). Studies on the Kunlun loess since the Holocene suggest that solar radiation is the main factor controlling dust activity (Tang et al., 2007; Teng et al., 2015). Some scholars (Machalett et al., 2008; Fitzsimmons et al., 2020) suggested that dust activity along the northern piedmont belts of western Tianshan Mountains in southeastern Kazakhstan is mainly controlled by the Asiatic polar front. However, another study of dust activity in southern Kazakhstan suggests that the advance of the Tianshan Mountain glaciers led to an increase in dust activity during the MIS3 (Fitzsimmons et al., 2018), and there is also a study that considers the Siberian High as the main driving force of southern Kazakhstan dust activity since 14.4 kyr (Su et al., 2023). For the Ili basin, several factors have been recommended for the loess deposit. Siberian High is the main contributor to the dust activities in the eastern Ili Basin (Cheng et al., 2021; 2022; Kang et al., 2022); It is also suggested that more factors should be considered (Li et al., 2016b, 2021a; Song et al., 2018; Prud'homme et al., 2021; Li et al., 2022a, 2023). For example, Li et al. (2023) suggested that the change of westerly wind intensity and water vapor transport intensity caused by obliquity and precession are the main factors determining activity in the Ili Basin since the late Pleistocene; Cheng et al. (2020) used the KETB loess profile suggest that glaciers developed in the Tianshan Mountains during the MIS3b affected dust activity in the Ili Basin. The studies of mechanisms of dust activity in Central Asia have different understandings in various regions during different periods. Therefore, it is important to reconstruct a synthetic record of Central Asian dust activity to clarify the main controlling factor of Central Asian dust activity.

In this study, we synthesized Mean Grain Size (MGS) data from 12 loess profiles and geochronological data from 42 profiles in Central Asia with robust radiometric dating including Optically Stimulated Luminescence (OSL) and Accelerator Mass Spectrometry (AMS) ^{14}C to calculate the DAR of each loess profile. And we normalized and overlapped the DAR and MGS data with the Z-score method, and tried to reconstruct dust activity and discuss the controlling factors in Central Asia. Our study will contribute to a comprehensive understanding of spatial-temporal variations in dust activity during loess depositional processes across Central Asia since 80 kyr ago.

2. Study Area, Materials and Methods

2.1. Study area

Central Asia is a vast arid region located at the heart of the Eurasian continent, characterized by diverse geographical features. It is surrounded by mountain ranges, including the Altai Mountains to the north, the Alborz, Hindu Kush, and Pamir Mountains to the south (Fig. 1). These mountains not only shape the landscape but also influence the climate and ecosystems of the region. The Central Asian region extends from the Caspian Sea in the west to Xinjiang, China in the east. Intermountain basins are scattered throughout the western and southern parts of Central Asia, including the Tajik, Junggar, Fergana, Ili, and Tarim basins. The western part of Central Asia is characterized by plains, and deserts are widespread in the region. Notable deserts in Central Asia include the Karakum, Kyzlkum, Muyunkum and Taklimakan deserts.

The climate of Central Asia is a typical continental temperate dry climate, which is characterized by a hot summer and cold winter, and the seasonal difference in precipitation is very large (Song et al., 2021). The moisture advection controlled by the mid-latitude westerlies, the Siberian High, and the front Asiatic polar front has a great impact on the climate system in Central Asia (Vandenberghe et al., 2006;Machalett et al., 2008; Feng et al., 2011; Huang et al., 2015; Li et al., 2019b). When the Asiatic polar is stronger, it causes strong cyclonic storms and aeolian transport over Central Asia, leading to dust activity (Machalett et al., 2008). The Siberian High, closely related to the East Asian winter monsoon, creates low-level atmospheric winds, providing wind power for dust activities (Kang et al., 2022). The East Asian summer monsoon and the Indian monsoon exert a limited impact on eastern and southern Central Asia (Chen et al., 2019). The high mountains in Central Asia act as barriers that capture moisture carried by the Westerlies, which significantly influences regional climate and environment (Caves Rugenstein and Chamberlain, 2018). Precipitation in Central Asia is mainly controlled by the westerlies, along the windward slopes of the high mountains, the ascent of the Westerly air mass at higher elevations leads to topographic rain, resulting in abundant precipitation. Conversely, the intermountain basins and the leeward slopes experience less precipitation. This topographical effect plays a crucial role in shaping the distribution of rainfall across the region (Song et al., 2021).

2.2. Material

In this study, we selected loess profiles to calculate DAR according to the following criteria: (1) The profiles must be composed of typical aeolian loess without secondary modification by humans or fluvial or gravity-driven processes. (2) Profiles have independent reliable data including OSL and AMS ^{14}C ages. (3) Profiles older than 50 kyr have an age control point every 15 kyrs, while younger profiles have one within 10 kyrs. (4) To avoid the influence of dating methods, we use a single dating method uniformly for each subregion. Following these criteria, we chose chronological data from 42 loess profiles across the entire study region to explore changes in DAR in Central Asia (Table S1). We also selected 12 profiles for the study of Mean Grain Size (MGS) based on the publicly available grain size data of loess profiles in Central Asia (Table S1).

2.3. Methods

Among these selected profiles, 38 loess profiles contain OSL data, and the remaining 4 loess profiles are AMS ^{14}C data, as detailed in Table S1. If the reported profiles have Bayesian age data, we use them directly in this study. Otherwise, we use Bacon 2.3 program to process the dating results of the selected 30 loess profiles, and establish the Bayesian age-depth model (Blaauw and Christen, 2011) with the resolution of 2 cm. While executing the program, we set the parameters to "thick = 10″ and use the recommended value for "acc.mean". If the data

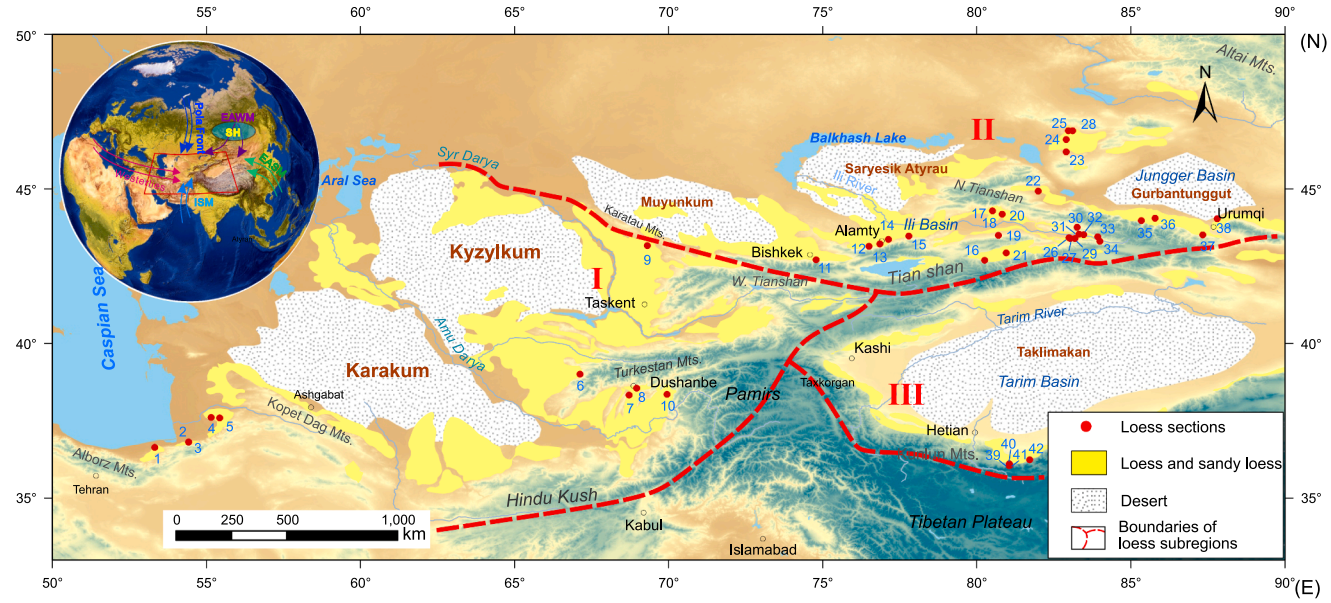

Fig. 1. Distribution of loess and desert in Central Asia with involved loess profiles (modified from Song et al. (2021)). The numbers and red solid points represent the involved loess profile in this study. The upper left insert figure depicts the main atmospheric circulation systems influencing the Central Asia. ISM: Indian Summer Monsoon; EAWM: East Asian Winter Monsoon; EASM: East Asian Summer Monsoon; SH: Siberian High. (For interpretation of the references to colour in this figure legend, the reader is referred to the web version of this article.) 1-Neka (Kehl et al., 2021); 2-Toshan19 (Li et al., 2025); 3-Toshan (Lauer et al., 2017a); 4-Agh Band (Lauer et al., 2017b); 5-YBD (Wei et al., 2021); 6-Rudak (Zhang et al., 2020); 7-TJK (Tian et al., 2021); 8-KP (Yang et al., 2020b); 9-VAL (Fitzsimmons et al., 2017); 10-Hoalin (Wang et al., 2018); 11-NRO (Youn et al., 2014); 12-MBK (Fitzsimmons et al., 2017); 13-REM (Fitzsimmons et al., 2018); 14-PAN (Dave et al., 2023); 15-ASH (Dave et al., 2023); 16-ZSP (Song et al., 2018); 17-QSH (Zhang et al., 2023); 18-QSH24 (Li et al., 2024); 19-DHS (Li et al., 2024); 20-SGX (Sun et al., 2020); 21-ZS (Kang et al., 2020b); 22-SG18 (Yang et al., 2021); 23-YM (Li et al., 2019a); 24-AK (Li et al., 2024); 25-TC (Li et al., 2019a); 26-XEB (Kang et al., 2020b); 27-TLD (Kang et al., 2020b); 28-KETB (Cheng et al., 2022); 29-XY17 (Li et al., 2020); 30-NLK (Li et al., 2018b); 31-ZKT(E, C.Y. et al., 2012); 32-TEG (Zhang et al., 2023); 33-KS15 (Li et al., 2018a); 34-NLT17 (Li et al., 2020); 35-LJW10 (Li et al., 2015); 36-QS16 (Li et al., 2020); 37-URS (Lu et al., 2016); 38-BYH10 (Li et al., 2016a); 39-KLB (Pan, 2013); 40-KY (Fan et al., 2023b); 41-KLA (Pan, 2013); 42-KMA (Tang et al., 2007).

overlap with the age-depth model by less than 90 %, we will adjust the program parameters appropriately to ensure the high reliability of the Bayesian age data.

We determine the DAR in meters per thousand years (m/kyr) by calculating the first derivative of the age-depth curve for each loess section. Additionally, we utilized the Z-Score method to standardize the DAR and the MGS sequences (Kreyszig, 1979). The Z-Score transform is a statistical method that standardizes a dataset by expressing each data point's deviation from the mean in terms of standard deviations, represented by the formula $(x-\mu)/\sigma$, where "x" is the data point, "μ" is the mean, and "σ" is the standard deviation. This transformation results in unitless Z-Score scores, providing a standardized scale for comparison and analysis across different datasets. This process enhances data uniformity and facilitates meaningful comparisons. Here, the normalized formula is $DAR_{normalized}=(DAR-DAR_{mean})/DAR_{standard\ deviation}$ and $MGS_{normalized}=(MGS-MGS_{mean})/MGS_{standard\ deviation}$. Calculating the $DAR_{normalized}$ (DAR_n) and $MGS_{normalized}$ (MGS_n) of each loess profile at a 0.5 kyr resolution. Due to the interference of dating techniques and human activities, we removed the DAR_n and MGS_n data within the last 1 kyr (Kang et al., 2022).

We follow the subdivision principles outlined by Song et al. (2021) to delineate the Central Asian subregions (Fig. 1). **Subregion I (the Western part of Central Asia)**: Encompassing the western expanse of Central Asia, this arid core area stretches from the Caspian Sea to the Western Tianshan and Pamir Plateau, covering regions in Northern Iran, Turkmenistan, Tajikistan, Uzbekistan, and the southern parts of Kyrgyzstan. **Subregion II (the Northern part of Central Asia)**: Situated north of the Tianshan Mountains, this area extends into southeastern Kazakhstan, including the Ili Basin, Tacheng Basin, and the Altai region in Xinjiang, China. **Subregion III (the Eastern part of Central Asia)**: Covering the Tarim Basin and its surrounding areas, which comprises the Taklamakan Desert and Lop Nor.

3. Results

3.1. Subregion I

Subregion I spans from the Caspian Sea to the west Tianshan Mountains and Pamirs Plateau(Song et al., 2021). We calculated the DAR of 10 loess profiles(Fitzsimmons et al., 2017; Lauer et al., 2017a,b; Wang et al., 2018; Yang et al., 2020b; Zhang et al., 2020; Kehl et al., 2021; Tian et al., 2021; Wei et al., 2021; Li et al., 2025) since 80 kyr ago, and all profiles chronological data are OSL (Table S1). The thickness of the loess profiles in this subregion range from 4 to 54 m. Among these profiles, the Agh Band profile in Iran (Lauer et al., 2017b) exhibits the highest average DAR at 1.05 m/kyr, while the Rudak section in Uzbekistan (Zhang et al., 2020) has the lowest average DAR at 0.06 m/kyr (Table S1). The DAR variation of glacial and interglacial periods in this subregion is not obvious. The DAR values for the Neka (Kehl et al., 2021), Toshan (Lauer et al., 2017a), and TJK (Tian et al., 2021) profiles during MIS 3 are notably higher compared to other periods. For the KP (Yang et al., 2020b), TJK (Tian et al., 2021), and Hoalin (Wang et al., 2018) profiles, the DAR values during MIS 2 are elevated above those of MIS 1 (Fig. 2).

We normalized the DARs of all loess profiles in this subregion using Z-scores method. It can be found that the DAR_n increases gradually from MIS5 to MIS3, and the DAR_n is the highest at MIS3 (Fig. 3). At approximately 57 kyr, there was a significant fluctuation characterized by a sudden decrease followed by an increase. DAR_n reached its peak at around 42 kyr, gradually decreasing with fluctuations thereafter. There was a sudden increase during the middle and late Holocene.

3.2. Subregion II

This subregion is located northern part of the Tianshan Mountains

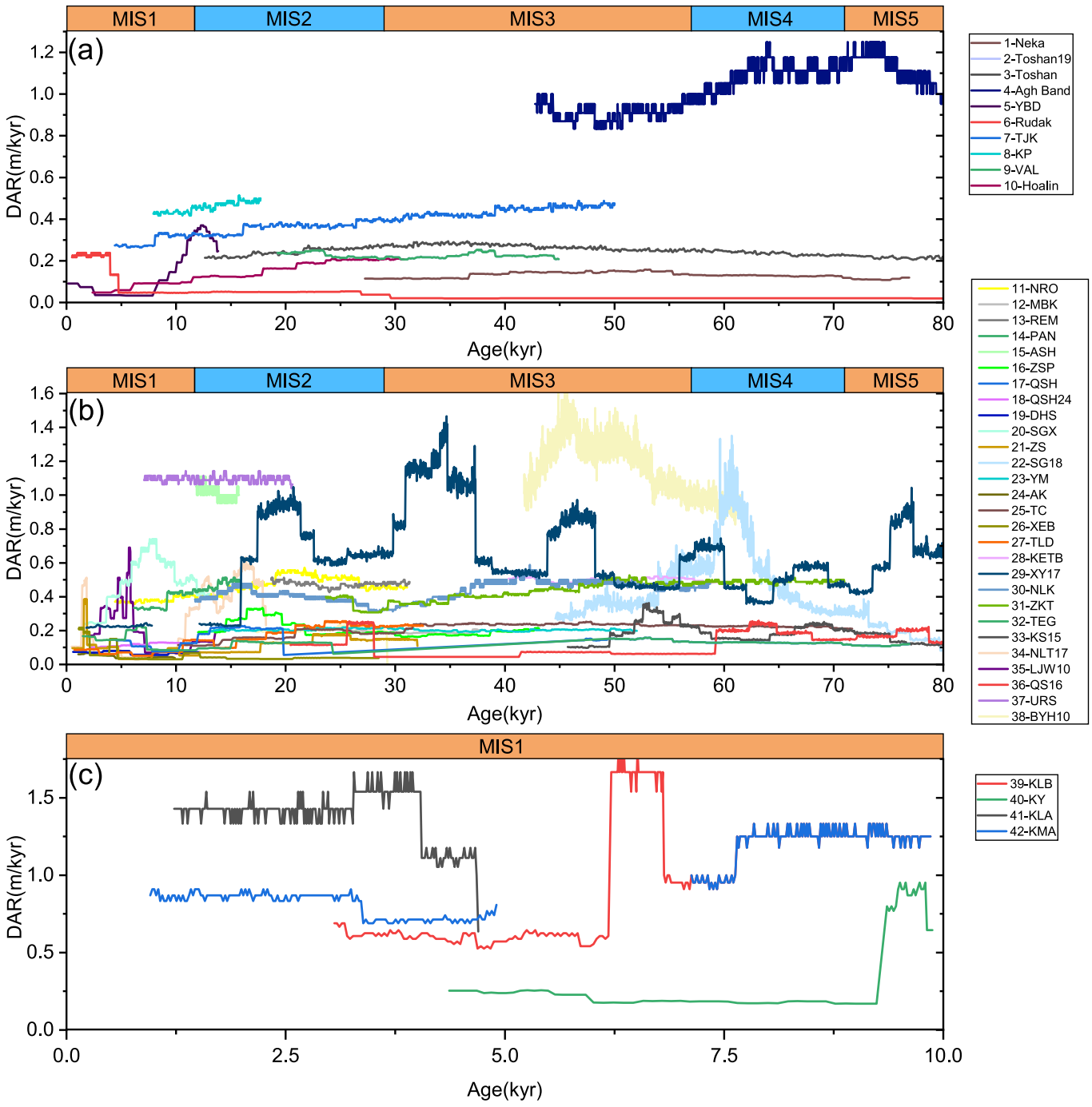

Fig. 2. DAR variations of loess profiles in Central Asia. (a) Subregion I (b) Subregion II. (c) Subregion III.

and the Altai region of Xinjiang Province, China (Song et al., 2021). Total 28 loess profiles with OSL data were selected for DARs determination (Table S1). Profiles ASH in Kazakhstan (Dave et al., 2023) exhibit the highest average DAR at 1.02 m/kyr. In contrast, the profile XEB in the Ili Basin (Kang et al., 2020b) has the lowest average DAR at 0.07 m/kyr (Table S1).

The DAR of the NLK (Li et al., 2018b), XY17 (Li et al., 2020) , BYH10 (Li et al., 2016a), and TC (Li et al., 2019a)profiles during MIS3 is higher than in other periods (Fig. 2). Specifically, the DAR values for NLK and XY17 during MIS3 are higher than those during MIS2 (Fig. 2). For the BYH10 profile, the DAR value during MIS3 is higher than that during MIS4 (Fig. 2). The TC profile shows a DAR value during MIS3 that is higher than those during both MIS2 and MIS4 (Fig. 2). The DAR values for profiles XY17, NRO (Youn et al., 2014), NLT17 (Li et al., 2020), ZS (Kang et al., 2020b), and PAN (Dave et al., 2023) are higher in MIS2 than in MIS1 (Fig. 2). For the XY17 profile, which is one of the longer sequences in this subregion, the DAR value in MIS3 is higher than in MIS2 and MIS4, and the DAR value in MIS2 is higher than in MIS4 (Fig. 2). Other than that, in the eastern Ili Basin, NLK and ZKT (E, C.Y. et al., 2012) profiles DAR values are very similar, NLK has a DAR of 0.49 m/kyr, while the ZKT profile, exhibits a DAR of 0.46 m/kyr (Table S1). And their DAR changes in both profiles remain consistent during the period from approximately 45 kyr to 25 kyr (Fig. 2).

The variation of DAR_n in this region is similar to that in subregion I, albeit with subtle differences (Fig. 3). DAR_n has shown a gradual increase since MIS5, reaching its peak at around 50 kyr. However, the

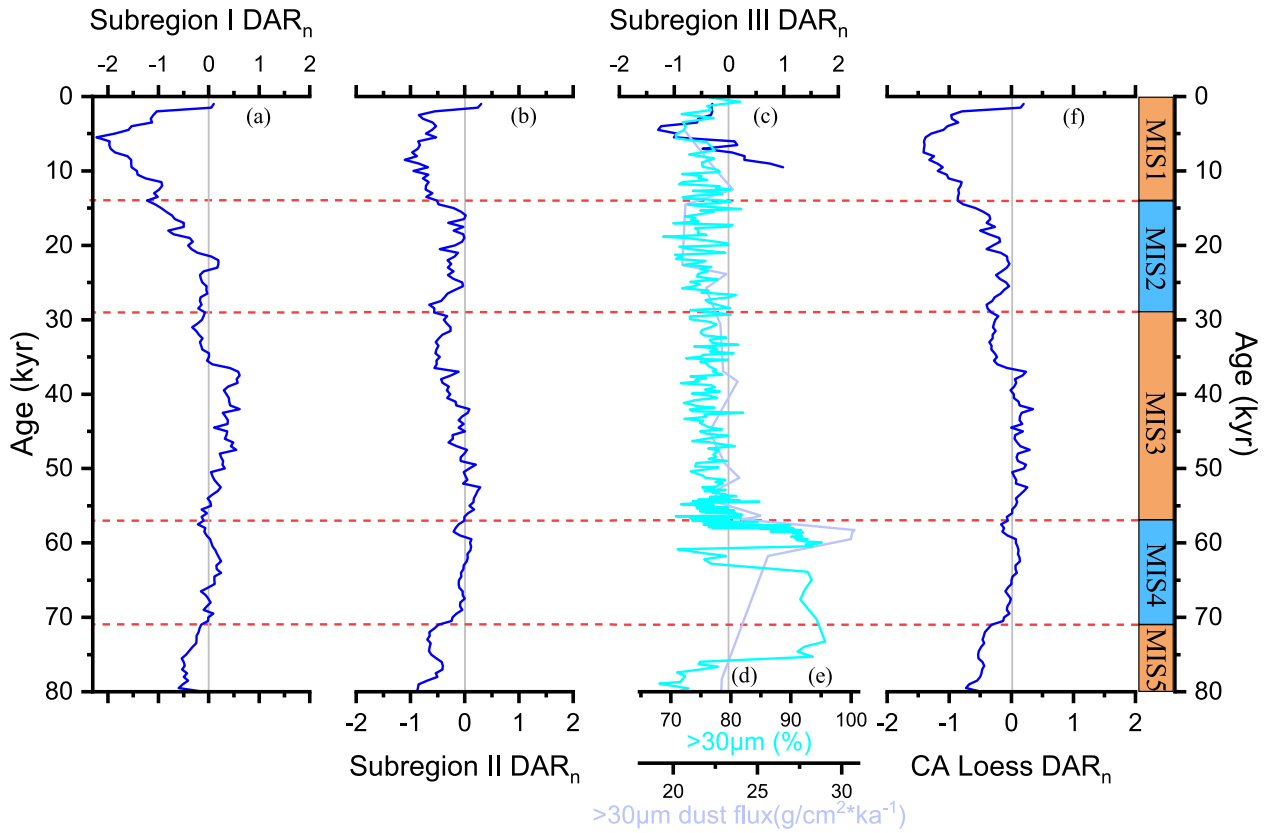

Fig. 3. DAR$_n$ changes of three subregions in Central Asia. (a) Subregion I (b) Subregion II. (c) Subregion III. (d and e) > 30 μm grain size and its flux of the loess core in the southern margin of the Tarim basin (Fang et al., 2020) (f) the average of subregion I and subregion II.

increment is not as substantial as observed in subregion I. The DAR$_n$ from MIS3 to early and middle Holocene generally shows a downward trend. However, there is a more significant increase in fluctuation during MIS2 compared to subregion I. DAR$_n$ increased in the middle and late Holocene, which is the same as the change of subregion I.

3.3. Subregion III

The chronological data for this subregion are the most limited, consisting of only 4 datasets (Tang et al., 2007; Pan, 2013; Fan et al., 2023b), with 4 on AMS ^{14}C. The loess in this subregion is mainly deposited in the foothills of the Kunlun Mountains, with relatively short loess sequences and generally higher DAR compared to the other two

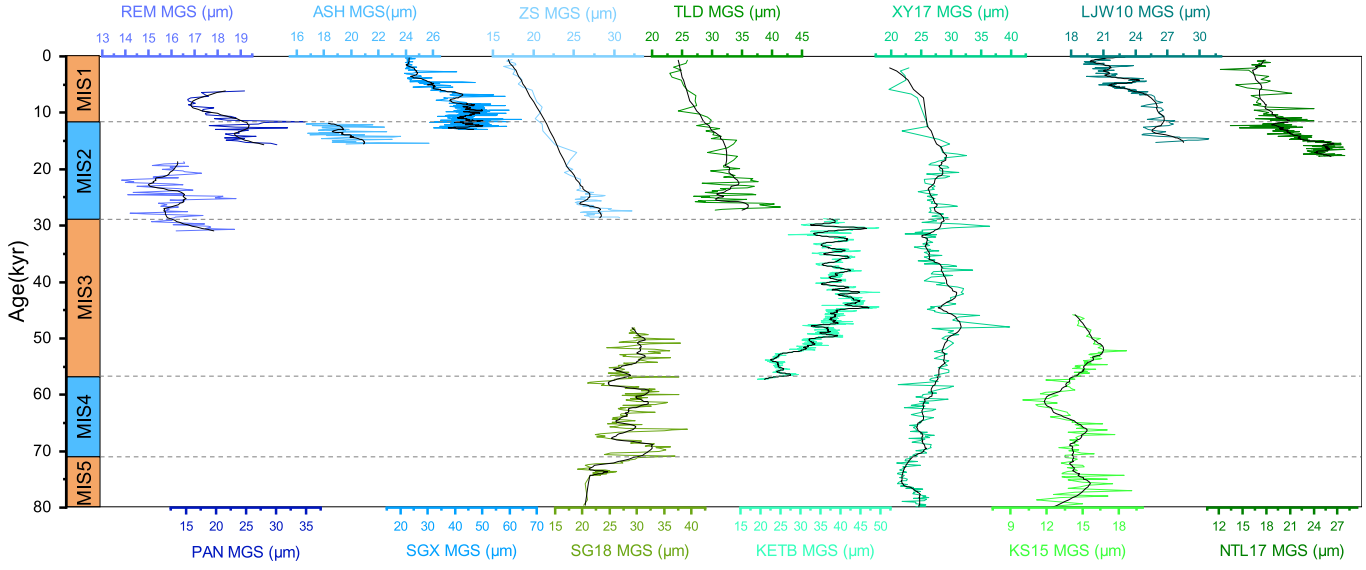

Fig. 4. Mean grain sizes of REM (Fitzsimmons et al., 2018), PAN (Dave et al., 2023), ASH (Dave et al., 2023), SGX (Sun et al., 2020), ZS (Kang et al., 2020b), SG18 (Yang et al., 2021), TLD (Kang et al., 2020b), KETB (Cheng et al., 2020), XY17 (Li et al., 2020), KS15 (Li et al., 2018a), LJW10 (Li et al., 2015), and NTL17 (Li et al., 2020) loess profiles.

subregions. Among them, the highest DAR value is the KLA profile (Pan, 2013) with 1.4 m/kyr, followed by the KLB profile (Pan, 2013) with 1.09 m/kyr, and the KMA profile (Tang et al., 2007) with 1.02 m/kyr (Table S1). The DAR in this subregion is generally low during the middle Holocene (Fig. 2). The DAR_n in this subregion generally shows a trend of decreasing and then increasing during the Holocene, reaching a minimum value around 5 kyr ago (Fig. 3).

3.4. Variation of Central Asian MGS

We have compiled the mean grain size sequences of 12 loess profiles from Central Asia (Table S1). We can find that the SG18 (Yang et al., 2021), KS15 (Li et al., 2018a), and XY17 (Li et al., 2020) profiles exhibit larger MGS during the MIS 3, and the XY17, KS15, and KETB (Cheng et al., 2022) profiles reach a peak around 50 kyr ago (Fig. 4). ZS, TLD, LJW10 and NTL17 show a trend of gradually decreasing MGS from MIS 2 to MIS 1. All profiles collectively exhibit a trend of increasing MGS from MIS 5 to mid-MIS 3, followed by a gradual decrease in MGS up to MIS 1 (Fig. 4).

4. Discussion

4.1. Advantages of Z-score for DAR and MGS

The Z-score method offers advantages by standardizing and comparing various variables by transforming raw values into unitless scores, facilitating the synthesis of multiple indicators, and enabling large-scale spatial analyses while mitigating the influence of local factors. In this study, the Z-score transforms DAR data into unitless scores, which is crucial for ensuring consistency in the interpretation of dust-related variables. The method is effective in synthesizing various indicators related to dust accumulation. This capability enables researchers to integrate diverse sources of information, providing a more comprehensive understanding of dust dynamics. It has been successfully applied in the synthesis of multiple indicators in loess studies in the Ili Basin (Li et al., 2022b) and Loess Plateau (Zhao et al., 2022). Due to the influence of topographic factors, there are some inconsistencies in Central Asian loess in space (Yang et al., 2020a). The influence of topographic and other localized factors cannot be overlooked in the study of local loess accumulation. However, when considered across geological timescales, such environmental parameters are generally regarded as relatively stable background variables. By applying Z-score normalization, we systematically eliminate interference from these long-term static variables in the dataset, thereby amplifying climate-driven signals and sedimentodynamic information that exhibit significant variations over long timescales. This methodological approach establishes a refined data framework for deciphering regional environmental evolution patterns, while enhancing the interpretability of sedimentary processes within a spatiotemporal continuum.

4.2. Trend of DAR_n, MGS_n and other indicators

Based on DAR_n analysis of each region, we observed a consistent pattern of change in subregions I and II, albeit with slight differences (Fig. 4a, b). This similarity suggests a shared mechanism governing DAR_n fluctuations in these two subregions. Despite the limited chronological data for subregion III, the DAR_n changes are also similar to the other two subregions (Fig. 4a, b, c), suggesting that the driving mechanisms of dust activity in this subregion may be the same as in the other two subregions. Due to the limited chronological data in the subregion III, which is based on ^{14}C dating, we have combined the DAR_n from subregions I and II to represent the DAR_n changes in Central Asia.

We can observe that the changes in Central Asian MGS_n and DAR_n are synchronized; when DAR_n is high, MGS_n also becomes coarser, and vice versa, it becomes finer (Fig. 5a, b). This is consistent with the traditional understanding of loess research, where higher dust activity corresponds to higher sedimentation rates and coarser loess particle sizes, and vice versa (Li et al., 2019b). This indicates that MGS_n and DAR_n effectively reflect the intensity of dust activity in Central Asia. To find the possible control factors, we compare Central Asian MGS_n and DAR_n with precession, obliquity (Laskar et al., 2004), NGRIP ice core $\delta^{18}O$ (Andersen et al., 2004), the periods of glacier duration of Tianshan Mountain (Zhao et al., 2009; Li et al., 2014), NLK (Nilka) loess profile sand fraction(Li et al., 2019b), Rel_{Hm+Gt} of Core LV63-4–2 (Zhong et al., 2024) and the MGS of the Jing Yuan (JY) loess profile (Sun et al., 2010) (Fig. 5).

The Central Asian DAR_n and MGS_n correlate closely with the JY MGS and the NGRIP ice core $\delta^{18}O$ after 40 kyr (Andersen et al., 2004; Sun et al., 2010). Both DAR_n, MGS_n and JY MGS gradually increased from around 35 kyr to the middle of MIS2, declined until the middle Holocene, and then DAR_n and JY MGS increased again, MGS_n declined (Fig. 5a, b, i). However, this trend reversed before approximately 35 kyr, with DAR_n, MGS_n, are different from JY MGS (Fig. 5a, b, i). During this period, DAR_n and MGS_n had high values around 35 to 53 kyr, while JY section MGS decreased from around 35 to 50 kyr and then increased (Fig. 5a, b, i). Notably, trends of DAR_n and MGS_n diverge from NGRIP ice core $\delta^{18}O$ values (Andersen et al., 2004) between 35 and 53 kyr where DAR_n and MGS_n have high value while ice core $\delta^{18}O$ decreases (Fig. 5a, b, g). MGS_n, DAR_n and NGRIP ice core $\delta^{18}O$ changes align in other periods. Conversely, the trends of DAR_n and MGS_n are broadly similar to those of the NLK sand fraction and $Rel_{Hm+Gt,}$ of Core LV63-4–2 with peaks occurring during MIS 2, MIS 3, and MIS 4 (Li et al., 2019b; Zhong et al., 2024) (Fig. 5a, b, c, h). The sand fraction of the NLK profile, serving as an effective indicator of regional dust activity, shows significant correlations with DAR_n and MGS_n. This indicates that the synthetic dataset can accurately reflect the spatio-temporal variation characteristics of regional dust activities in central Asia. Also, trends of DAR_n and MGS_n are consistent with the change trend of precession (Fig. 5a, b, d). DAR_n and MGS_n from 35 to 53 kyr showed a high value, there were large-scale glacier activities in the central and western Tianshan Mountains (Zhao et al., 2009; Li et al., 2014), and corresponding to high precession and high inclination during this period (Laskar et al., 2004) (Fig. 5a, b, f).

4.3. Possible mechanisms of dust activity in Central Asia

Previous studies (Tang et al., 2007; Teng et al., 2015) propose that the loess of subregion III is driven by the intensity of the Northern Hemisphere westerlies, which is forced by solar radiation. Meanwhile, the driving mechanisms in subregions I and II appear to be linked to the Siberian High, westerlies, and Asiatic polar front (Machalett et al., 2008; Kang et al., 2022; Li et al., 2023). To address the temporal coverage limitations of DAR_n records in subregion III (currently restricted to Holocene data), we supplemented the dataset with $>$ 30 μm particle fraction and its dust flux indices from Fang et al. (2020) loess core stratigraphy. This multi-proxy approach enables robust validation of dust activity patterns in subregion III over the past 80 kyr. We can find that the changes of core records and DAR_n of subregion III since the Holocene have been consistent. Also, from 80 kyr to the Holocene, the core records of this partition show a high degree of synchronicity with the sedimentary trends of the subregions I and II. The mechanism governing dust accumulation in subregion III may be similar to those of subregions I and II. Given the relatively limited temporal coverage of sedimentary records in subregion III, we refrain from extensive discussion on this aspect in the present article.

Central Asian loess predominantly comprises deposits from proximal material deposits (Li et al., 2023). When the climate in the source area turns dry and cold, the vegetation coverage reduces, resulting in increasing susceptibility to wind erosion, leading to heightened dust activity (Li et al., 2023). Changes in the water vapor transport of the westerlies intense played a role in the alterations between dry and wet environments in Central Asia (Li et al., 2020). Li et al. (2023) proposed that high (low) obliquity and high (low) precession will cause the

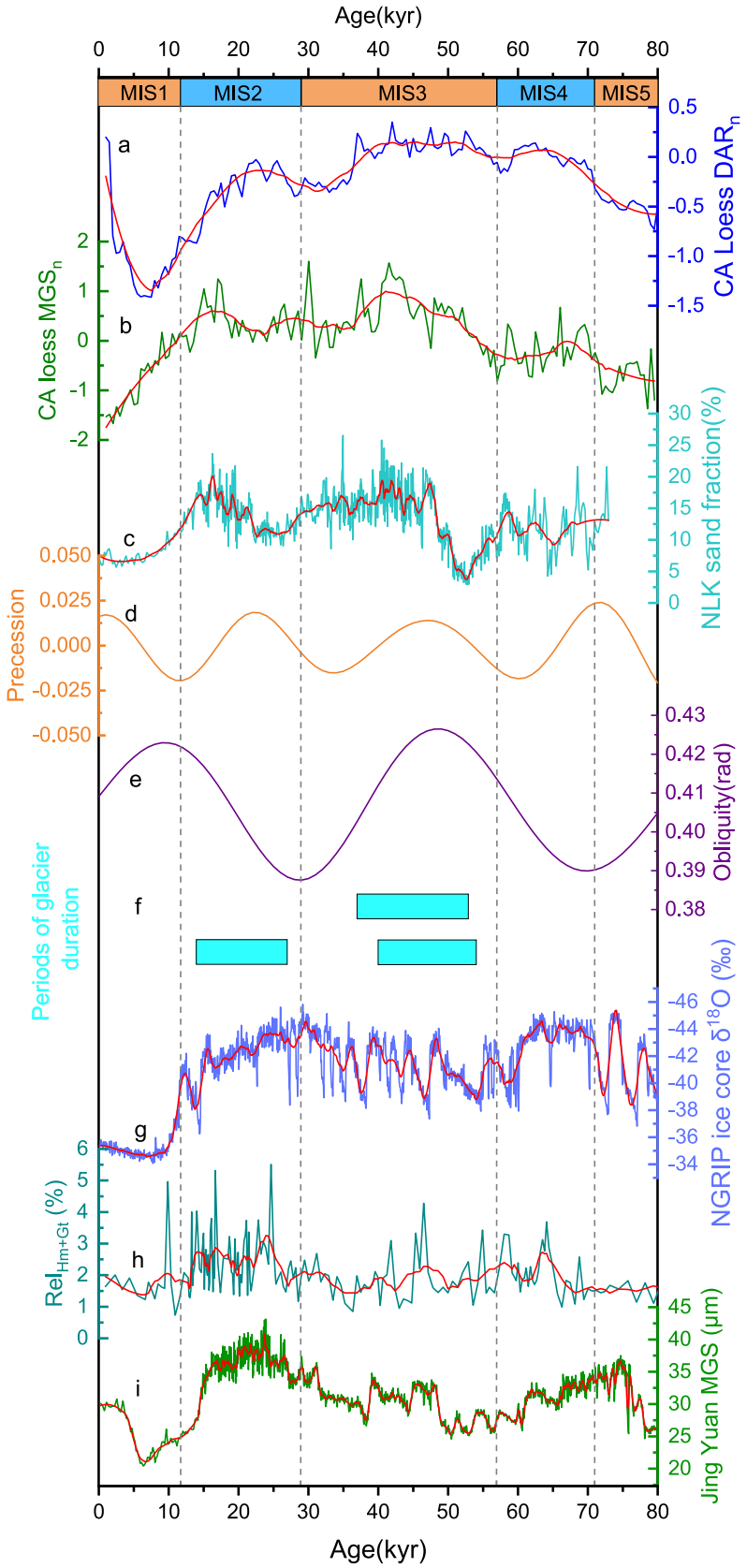

Fig. 5. The comparison of DAR_n of subregion I and II with other proxies. (a) MGS_n of Central Asian loess (b) DAR_n of Central Asian loess (c) NLK (Nilka) loess profile sand fraction(Li et al., 2019b). (d) precession(Laskar et al., 2004). (e) obliquity(Laskar et al., 2004). (f) the periods glacier duration(Zhao et al., 2009; Li et al., 2014). (g) the NGRIP ice core $\delta^{18}O$(Andersen et al., 2004). (h) Rel_{Hm+Gt} of Core LV63-4–2(Zhong et al., 2024) (i) the mean grain sizes (MGS) of the Jing Yuan (JY) (Sun et al., 2010) (red line: moving average). (For interpretation of the references to colour in this figure legend, the reader is referred to the web version of this article.)

weakening (enhancement) of the westerlies intensity, which will weaken (enhance) the water vapor activity. Therefore, DAR_n and MGS_n have the highest value during the ~ 35 to 53 kyr period with high precession and high obliquity (Laskar et al., 2004). The trends of precession, obliquity, DAR_n, and MGS_n, suggest that changes in water vapor influenced by the westerlies due to precession and obliquity play a significant role in dust activity in Central Asia.

Precession and obliquity also control the change of global ice volume, which influences the strength of the Siberian High (Kang et al., 2020a). Siberian High not only affects the dry and wet changes in Central Asia but also produces near-surface wind to provide wind power for dust emission in Central Asia (Kang et al., 2022; Li et al., 2023). From the comparison of the trends of NGRIP $\delta^{18}O$, MGS of JY section and NLK sand fraction with DAR_n and MGS_n (Fig. 5a, b, c, i), it can be found that when the High-latitude temperatures in the Northern Hemisphere decreases (the $\delta^{18}O$ value become more negative), the Siberian High-intensity increases (MGS of JY is coarse), DAR_n and MGS_n increases. The strengthening of the Siberian High induces dry climate conditions and intense near-surface winds, thereby enhancing dust activity in Central Asia (Kang et al., 2022). However, during the MIS3, DAR_n and MGS_n exhibited an opposite trend to that of NGRIP $\delta^{18}O$ and the MGS of JY (Fig. 5a, b, g, i), suggesting that the Siberian High might not have been the key factor driving dust activity in Central Asia during that phase.

Meanwhile, Central Asian loess DAR_n of MIS3 is higher than that of MIS2 and MIS4 (Fig. 5a). Changes in DAR_n during glacial and interglacial periods contradict the conventional understanding from prior studies, which posited that dry and cold conditions during glacial periods would result in increased DAR, while DAR would decrease in warm and wet interglacial periods (Ding et al., 2002; Dodonov and Baiguzina, 1995; Ujvari et al., 2017). Therefore, dust activity in Central Asia was controlled by other factors during the MIS3 period.

Previous investigations into glacier activity in the central and western Tianshan Mountains indicate significant large-scale glacier activity in the region during the MIS3b substage (Zhao et al., 2009; Li et al., 2014). During the MIS3b substage, the glacier activity in the central and western Tianshan Mountains was not synchronized with global ice volume changes (Cheng et al., 2020). The stronger dust activity in Central Asia aligns with the period of glacier activity in the Tianshan area. Consequently, the presence of large-scale glaciers in the Tianshan Mountains as a cold high-pressure system influences the Central Asian near-surface wind, thereby intensifying dust activity in Central Asia (Kutzbach and Wright, 1985; Bartlein et al., 1998; Isarin and Renssen, 1999). Therefore, during the MIS3, the decrease in westerly moisture transport due to high precession and obliquity, along with the glacier activity in the Tianshan Mountains, were the critical factors leading to the increased dust activity in Central Asia.

Combining the indicator of dust input in the North Pacific Ocean (Rel_{Hm+Gt} Core LV63-4–2), we can discern that during the MIS2 phase, large-scale dust activity in East and Central Asia led to greater dust input into the North Pacific compared to other periods (Zhong et al., 2024) (Fig. 5a, b, h). During the MIS3 and MIS4, Central Asia predominantly served as the major source region for dust activity (Sun et al., 2010; Zhong et al., 2024). The Rel_{Hm+Gt} indicates a reduction in dust input compared to the MIS2, but it remains significantly elevated (Fig. 5h). The volume of dust input into the North Pacific aligns with and substantiates our research outcomes on dust activity in Central Asia (Zhong et al., 2024).

In summary, the variations in the climate system in Central Asia induced by westerly intense which controlled by precession and obliquity influence water vapor and wind power changes since the late Pleistocene, thereby impacting dust activity in Central Asia. Additionally, Siberian High and local large-scale glacier activities in the region also play a role in driving dust activity.

5. Conclusion

In this study, we calculate DAR of Central Asian loess profiles and employ Z-score to normalize loess DAR and MGS to investigate the patterns of sediment and dust activity in Central Asia. Our findings led to the following conclusions: In subregions I and II, DAR increased from MIS5 to MIS3, peaked during MIS3, declined from MIS3 to mid-Holocene, and increased again post-mid-Holocene. In subregion III, the variation of DAR has been more consistent with the other two subregions since the Holocene. The trend of loess DAR in all subregions exhibits remarkable similarity, suggesting that the primary controlling factors of all subregions are identical. The trends of Central Asian loess DAR and MGS are consistent, effectively reflecting the Central Asian dust activity since ~ 80 kyr ago. The dust activity in Central Asia is primarily driven by westerlies controlled by precession and obliquity, which in turn affects water vapor and wind power. Additionally, dust activity in Central Asia are also related to Siberian High and local glacier activities.

Data Availability

All new data are available in the Loess Science Date Center: https://www.lsdc.ac.cn/portal/data/2335.

CRediT authorship contribution statement

Haoru Wei: Writing – review & editing, Writing – original draft, Visualization, Methodology, Investigation, Formal analysis, Data curation, Conceptualization. **Yougui Song:** Writing – review & editing, Supervision, Resources, Funding acquisition, Conceptualization. **Yanping Wang:** Writing – original draft, Visualization, Software, Resources. **Mingyu Zhang:** Writing – review & editing, Validation, Formal analysis. **Hamid Gholami:** Methodology, Data curation. **Shugang Kang:** Writing – review & editing, Methodology. **Yue Li:** Investigation, Formal analysis. **Shukhrat Shukurov:** Methodology. **Nosir Shukurov:** Validation. **Rustam Orozbaev:** Methodology.

Declaration of competing interest

The authors declare that they have no known competing financial interests or personal relationships that could have appeared to influence the work reported in this paper.

Acknowledgements

This study supported by Natural Science Foundation of China (Nos: 42372220, 42172207, 42472254), the Science and Technology Innovation Project of Laoshan Laboratory (No: LSKJ202203300), the Youth Innovation Promotion Association Chinese Academy of Sciences (Y2022102) and the International Partnership Program of the Chinese Academy of Sciences.

Appendix A. Supplementary material

Supplementary data to this article can be found online at https://doi.org/10.1016/j.gr.2025.03.020.

References

Andersen, K.K., Azuma, N., Barnola, J.M., Bigler, M., Biscaye, P., Caillon, N., Chappellaz, J., Clausen, H.B., DahlJensen, D., Fischer, H., Flückiger, J., Fritzsche, D., Fujii, Y., Goto-Azuma, K., Gronvold, K., Gundestrup, N.S., Hansson, M., Huber, C., Hvidberg, C.S., Johnsen, S.J., Jonsell, U., Jouzel, J., Kipfstuhl, S., Landais, A., Leuenberger, M., Lorrain, R., Masson-Delmotte, V., Miller, H., Motoyama, H., Narita, H., Popp, T., Rasmussen, S.O., Raynaud, D., Rothlisberger, R., Ruth, U., Samyn, D., Schwander, J., Shoji, H., Siggard-Andersen, M.L., Steffensen, J.P., Stocker, T., Sveinbjörnsdóttir, A.E., Svensson, A., Takata, M., Tison, J.L., Thorsteinsson, T., Watanabe, O., Wilhelms, F., White, J.W.C., Project, N.G.I.C., 2004.

High-resolution record of Northern Hemisphere climate extending into the last interglacial period. Nature 431, 147–151.
Bartlein, P.J., Anderson, K.H., Anderson, P.M., Edwards, M.E., Mock, C.J., Thompson, R. S., Webb, R.S., Whitlock, C., 1998. Paleoclimate simulations for North America over the past 21,000 years: Features of the simulated climate and comparisons with paleoenvironmental data. Quat. Sci. Rev. 17, 549–585.
Blaauw, M., Christen, J.A., 2011. Flexible Paleoclimate Age-Depth Models Using an Autoregressive Gamma Process. Bayesian Anal. 6, 457–474.
Caves Rugenstein, J.K., Chamberlain, C.P., 2018. The evolution of hydroclimate in Asia over the Cenozoic: A stable-isotope perspective. Earth-Sci. Rev. 185, 1129–1156.
Chen, F.H., Chen, J.H., Huang, W., Chen, S.Q., Huang, X.Z., Jin, L.Y., Jia, J., Zhang, X.J., An, C.B., Zhang, J.W., Zhao, Y., Yu, Z.C., Zhang, R.H., Liu, J.B., Zhou, A.F., Feng, S., 2019. Westerlies Asia and monsoonal Asia: Spatiotemporal differences in climate change and possible mechanisms on decadal to sub-orbital timescales. Earth-Sci. Rev. 192, 337–354.
Cheng, L., Song, Y., Sun, H., Bradak, B., Orozbaev, R., Zong, X., Liu, H., 2020. Pronounced changes in paleo-wind direction and dust sources during MIS3b recorded in the Tacheng loess, northwest China. Quat. Int. 552, 122–134.
Cheng, L., Song, Y., Wu, Y., Liu, Y., Liu, H., Chang, H., Zong, X., Kang, S., 2021. Drivers for Asynchronous Patterns of Dust Accumulation in Central and Eastern Asia and in Greenland During the Last Glacial Maximum. Geophys. Res. Lett. 48, e2020GL091194.
Cheng, L., Song, Y., Yang, L., Chang, H., Wu, Y., Long, H., Miao, X., Dong, Z., 2022. Variations of the Intensity of the Siberian High During the Last Glacial Revealed by the Sorting Coefficient of Loess-Paleosol Deposits in Eastern Central Asia. Paleocean. Palaeoclimatol 37 (9), e2022PA004468.
Dave, A.K., Lisa, L., Scardia, G., Nigmatova, S., Fitzsimmons, K.E., 2023. The patchwork loess of Central Asia: Implications for interpreting aeolian dynamics and past climate circulation in piedmont regions. J. Quat. Sci. 38, 526–543.
Ding, Z.L., Ranov, V., Yang, S.L., Finaev, A., Han, J.M., Wang, G.A., 2002. The loess record in southern Tajikistan and correlation with Chinese loess. Earth Planet. Sci. Lett. 200, 387–400.
Dodonov, A.E., Baiguzina, L.L., 1995. Loess stratigraphy of Central Asia: Palaeoclimatic and palaeoenvironmental aspects. Quat. Sci. Rev. 14, 707–720.
Dodonov, A.E.J.G., 1991. Loess of Central Asia. GeoJournal 24, 9.
E, C.Y., Lai, Z.P., Sun, Y.J., Hou, G.L., Yu, L.P., Wu, C.Y., 2012. A luminescence dating study of loess deposits from the Yili River basin in western China. Quat. Geochronol. 10, 50–55.
Fan, Y., Jia, J., Xia, D., Liu, Y., Jiang, B., Yang, J., Gao, F., Chen, J., 2023a. Southward shift of the Westerlies during Heinrich Event 2: Evidence from loess deposits in Central Asia. Palaeogeog. Palaeoclimatol. Palaeoecol. 630 (2023), 111815.
Fan, Y.J., Jia, J., Yu, J.N., Liu, Y., Liu, X., Zhao, L., Xia, D.S., 2023b. Bond events in the Tarim Basin: The loess record. Quat. Int. 643, 73–80.
Fang, X., An, Z., Clemens, S.C., Zan, J., Shi, Z., Yang, S., Han, W., 2020. The 3.6-Ma aridity and westerlies history over midlatitude Asia linked with global climatic cooling. Proc. Natl. Acad. Sci. U.S.A. 117, 24729–24734.
Feng, Z.D., Ran, M., Yang, Q.L., Zhai, X.W., Wang, W., Zhang, X.S., Huang, C.Q., 2011. Stratigraphies and chronologies of late Quaternary loess–paleosol sequences in the core area of the central Asian arid zone. Quat. Int. 240, 156–166.
Fitzsimmons, K.E., Iovita, R., Sprafke, T., Glantz, M., Talamo, S., Horton, K., Beeton, T., Alipova, S., Bekseitov, G., Ospanov, Y., Deom, J.-M., Sala, R., Taimagambetov, Z., 2017. A chronological framework connecting the early Upper Palaeolithic across the Central Asian piedmont. J. Hum. Evol. 113, 107–126.
Fitzsimmons, K.E., Nowatzki, M., Dave, A.K., Harder, H., 2020. Intersections between wind regimes, topography and sediment supply: Perspectives from aeolian landforms in Central Asia. Palaeogeogr. Palaeocl. 540, 109531.
Fitzsimmons, K.E., Sprafke, T., Zielhofer, C., Gunter, C., Deom, J.M., Sala, R., Iovita, R., 2018. Loess accumulation in the Tian Shan piedmont: Implications for palaeoenvironmental change in arid Central Asia. Quat. Int. 469, 30–43.
Huang, W., Chen, J.H., Zhang, X.J., Feng, S., Chen, F.H., 2015. Definition of the core zone of the “westerlies-dominated climatic regime”, and its controlling factors during the instrumental period. Sci. China-Earth Sci. 58, 676–684.
Isarin, R.F.B., Renssen, H., 1999. Reconstructing and modelling Late Weichselian climates: the Younger Dryas in Europe as a case study. Earth-Sci. Rev. 48, 1–38.
Jia, J., Liu, H., Gao, F., Xia, D., 2018. Variations in in the westerlies in Central Asia since 16 ka recorded by a loess section from the Tien Shan Mountains. Palaeogeog. Palaeoclimatol. Palaeoecol. 504, 156–161.
Kang, S., Wang, X., Wang, N., Song, Y., Liu, W., Wang, D., Peng, J., 2022. Siberian High Modulated Suborbital-Scale Dust Accumulation Changes Over the Past 30 ka in the Eastern Yili Basin. Central Asia. Paleocean., Palaeoclimatol. 37, e2021PA004360.
Kang, S.G., Du, J.H., Wang, N., Dong, J.B., Wang, D., Wang, X.L., Qiang, X.K., Song, Y.G., 2020a. Early Holocene weakening and mid- to late Holocene strengthening of the East Asian winter monsoon. Geology 48, 1043–1047.
Kang, S.G., Wang, X.L., Roberts, H.M., Duller, G.A.T., Song, Y.G., Liu, W.G., Zhang, R., Liu, X.X., Lan, J.H., 2020b. Increasing effective moisture during the Holocene in the semiarid regions of the Yili Basin, Central Asia: Evidence from loess sections. Quat. Sci. Rev. 246, 106553.
Kehl, M., Vlaminck, S., Kohler, T., Laag, C., Rolf, C., Tsukamoto, S., Frechen, M., Sumita, M., Schmincke, H.U., Khormali, F., 2021. Pleistocene dynamics of dust accumulation and soil formation in the southern Caspian Lowlands - New insights from the loess-paleosol sequence at Neka-Abelou, northern Iran. Quat. Sci. Rev. 253, 106774.
Kohfeld, K.E., Harrison, S.P., 2001. DIRTMAP: the geological record of dust. Earth-Sci. Rev. 54, 81–114.
Kreyszig, E., 1979. Advanced Engineering Mathematics (Fourth ed.). Wiley, Hoboken, p. 880.
Kutzbach, J.E., Wright, H.E., 1985. Simulation of the climate of 18,000 years BP: Results for the North American/North Atlantic/European sector and comparison with the geologic record of North America. Quat. Sci. Rev. 4, 147–187.
Laskar, J., Robutel, P., Joutel, F., Gastineau, M., Correia, A.C.M., Levrard, B., 2004. A long-term numerical solution for the insolation quantities of the Earth. Astron. Astrophys. 428, 261–285.
Lauer, T., Frechen, M., Vlaminck, S., Kehl, M., Lehndorff, E., Shahriari, A., Khormali, F., 2017a. Luminescence-chronology of the loess palaeosol sequence Toshan, Northern Iran – A highly resolved climate archive for the last glacial–interglacial cycle. Quat. Int. 429, 3–12.
Lauer, T., Vlaminck, S., Frechen, M., Rolf, C., Kehl, M., Sharifi, J., Lehndorff, E., Khormali, F., 2017b. The Agh Band loess-palaeosol sequence - A terrestrial archive for climatic shifts during the last and penultimate glacialeinterglacial cycles in a semiarid region in northern Iran. Quat. Int. 429, 13–30.
Li, D., Zhao, H., Xie, H., Sun, A., Khormali, F., Wang, X., Wang, Q., Lahijani, H., Nashli, H.F., Xu, Y., Chen, F., 2025. Loess-paleosol sedimentological characteristics in northern Iran since the last interglacial and their paleoenvironmental significance. Quat. Sci. Rev. 354, 109213.
Li, G.Q., Chen, F.H., Xia, D.S., Yang, H., Zhang, X.J., Madsen, D.B., Oldknow, C., Wei, H. T., Rao, Z.G., Qiang, M.R., 2018a. A Tianshan Mountains loess-paleosol sequence indicates anti-phase climatic variations in arid central Asia and in East Asia. Earth Planet. Sci. Lett. 494, 153–163.
Li, G.Q., Rao, Z.G., Duan, Y.W., Xia, D.S., Wang, L.B., Madsen, D.B., Jia, J., Wei, H.T., Qiang, M.R., Chen, J.H., Chen, F.H., 2016a. Paleoenvironmental changes recorded in a luminescence dated loess/paleosol sequence from the Tianshan Mountains, arid central Asia, since the Penultimate Glaciation. Earth Planet. Sci. Lett. 448, 1–12.
Li, G.Q., Wen, L.J., Xia, D.S., Duan, Y.W., Rao, Z.G., Madsen, D.B., Wei, H.T., Li, F.L., Jia, J., Chen, F.H., 2015. Quartz OSL and K-feldspar pIRIR dating of a loess/paleosol sequence from arid central Asia, Tianshan Mountains, NW China. Quat. Geochronol. 28, 40–53.
Li, G., Yan, Z., Song, Y., Fitzsimmons, K.E., Yi, S., Kang, S., E, C., Stevens, T., Lai, Z., Dave, A.K., Chen, C., Deng, Y., Yang, H., Wang, L., Zhang, X., Qin, C., Zhao, Q., Buylaert, J.-P., Lu, T., Wang, Y., Liu, X., Ling, Z., Chang, Q., Wei, H., Wang, X., Chen, F., 2024. A comprehensive dataset of luminescence chronologies and environmental proxy indices of loess-paleosol deposits across Asia. npj Clim. Atoms. Sci 7 (1), 7.
Li, G.Q., Yang, H., Stevens, T., Zhang, X.J., Zhang, H.X., Wei, H.T., Zheng, W.P., Li, L.J., Liu, X.J., Chen, J.H., Xia, D.S., Oldknow, C., Ye, W., Chen, F.H., 2020. Differential ice volume and orbital modulation of Quaternary moisture patterns between Central and East Asia. Earth Planet. Sci. Lett. 530, 115901.
Li, Y., Han, L., Li, X., 2024. Positive correlation between dust activity and humidity in arid Central Asia during the Holocene. Quat. Sci Rev 324, 108442.
Li, Y., Han, L., Liu, X., Song, Y., Wang, Y., 2021a. Correlation and anti-correlation of the Asian summer monsoon and westerlies during the. Gondwana Res. 91, 112–120.
Li, Y., Liu, G., Chen, Y., Li, Y., Harbor, J., Stroeven, A.P., Caffee, M., Zhang, M., Li, C., Cui, Z., 2014. Timing and extent of Quaternary glaciations in the Tianger Range, eastern Tian Shan, China, investigated using ^{10}Be surface exposure dating. Quat. Sci Rev 98, 7–23.
Li, Y., Song, Y., Fitzsimmons, K.E., Chang, H., Orozbaev, R., Li, X., 2018b. Eolian dust dispersal patterns since the last glacial period in eastern Central Asia: insights from a loess-paleosol sequence in the Ili Basin. Clim. past. 14, 271–286.
Li, Y., Song, Y., Kaskaoutis, D.G., Zan, J., Orozbaev, R., Tan, L., Chen, X., 2021b. Aeolian dust dynamics in the Fergana Valley, Central Asia, since ~30 ka inferred from loess deposits. Geosci. Front. 12, 101180.
Li, Y., Song, Y., Kaskaoutis, D.G., Zhang, X., Chen, X., Shukurov, N., Orozbaev, R., 2022a. Atmospheric dust dynamics over Central Asia: A perspective view from loess deposits. Gondwana Res. 109, 150–165.
Li, Y., Song, Y., Lai, Z., Han, L., An, Z., 2016b. Rapid and cyclic dust accumulation during MIS 2 in Central Asia inferred from loess OSL dating and grain-size analysis. Sci. Rep. 6, 32365.
Li, Y., Song, Y., Yin, Q., Han, L., Wang, Y., 2019a. Orbital and millennial northern mid-latitude westerlies over the last glacial period. Clim. Dyn. 53, 3315–3324.
Li, Y., Song, Y.G., Chen, X.L., Shi, Z.G., Kaskaoutis, D.G., Gholami, H., Li, Y.D., 2023. Late Pleistocene dynamics of dust emissions related to westerlies revealed by quantifying loess provenance changes in North Tian Shan Central Asia. Catena 227, 107101.
Li, Y., Song, Y., Li, X., Xie, X., Kaskaoutis, D.G., Aminov, J., Yatimov, S., 2024. Aeolian dust dynamics in southern Central Asia revealed by the multi-timescale loess records in southern Tajikistan. Geomorphology 467, 109461.
Li, Y., Song, Y.G., Qiang, M.R., Miao, Y.F., Zeng, M.X., 2019b. Atmospheric Dust Variations in the Ili Basin, Northwest China, During the Last Glacial Period as Revealed by a High Mountain Loess-Paleosol Sequence. J. Geophys. Res. Atmos. 124, 8449–8466.
Li, Y.D., Li, Y., Song, Y.G., Wei, H.R., Wang, Y.P., Shukurov, N., 2022b. Effective Moisture Evolution since the Last Glacial Maximum Revealed by a Loess Record from the Westerlies-Dominated Ili Basin. NW China. Atmosphere 13 (11), 1931.
Lu, H., Xu, Y., Niu, Y., Wang, Z., Wang, H., Zhao, J., Zhang, W., Zheng, X., 2016. Late Quaternary loess deposition in the southern Chaiwopu Basin of the northern Chinese Tian Shan foreland and its palaeoclimatic implications. Boreas 45, 304–321.
Machalett, B., Oches, E.A., Frechen, M., Zöller, L., Hambach, U., Mavlyanova, N.G., Marković, S.B., Endlicher, W., 2008. Aeolian dust dynamics in central Asia during the Pleistocene: Driven by the long-term migration, seasonality, and permanency of the Asiatic polar front. Geochem. Geophys, Geosyst, pp. 9(8), 1–22.
Maher, B.A., Prospero, J.M., Mackie, D., Gaiero, D., Hesse, P.P., Balkanski, Y., 2010. Global connections between aeolian dust, climate and ocean biogeochemistry at the present day and at the last glacial maximum. Earth-Sci. Rev. 99, 61–97.

Mayaud, J.R., Wiggs, G.F.S., Bailey, R.M., 2016. Characterizing turbulent wind flow around dryland vegetation. Earth Surf. Processes Landforms 41, 1421–1436.
Pan, Y., 2013. Holocene loess deposits and environmental changes on the northern slope of Kunlun Mountains, Xinjiang, China. Xinjiang Institute of Ecology and Geography Chinese Academy of Sciences, Urumqi.
Prud'homme, C., Scardia, G., Vonhof, H., Guinoiseau, D., Nigmatova, S., Fiebig, J., Gerdes, A., Janssen, R., Fitzsimmons, K.E., 2021. Central Asian modulation of Northern Hemisphere moisture transfer over the Late Cenozoic. Commun. Earth Environm. 2, 106.
Shu, P., Niu, D., Song, Y., Si, Y., Kang, S., Li, B., Zhou, W., An, Z., 2025. Dust emissions in the arid Asian interior and abrupt changes in midlatitude atmospheric circulation during the glacial-Holocene transition. Global Planet. Change 248, 104758.
Song, Y., Lai, Z., Li, Y., Chen, T., Wang, Y., 2015. Comparison between luminescence and radiocarbon dating of late Quaternary loess from the Ili Basin in Central Asia. Quat. Geochronol. 30, 405–410.
Song, Y., Li, Y., Cheng, L., Zong, X., Kang, S., Ghafarpour, A., Li, X., Sun, H., Fu, X., Dong, J., Mamadjanov, Y., Orozbaev, R., Shukurov, N., Gholami, H., Shukurov, S., Xie, M., 2021. Spatio-temporal distribution of Quaternary loess across Central Asia. Palaeogeog. Palaeoclimatol. Palaeoecol. 567, 110279.
Song, Y., Luo, D., Du, J., Kang, S., Cheng, P., Fu, C., Guo, X., 2018. Radiometric dating of late Quaternary loess in the northern piedmont of South Tianshan Mountains: Implications for reliable dating. Geol. J. 53, 417–426.
Su, C., Xu, Z., Zhang, D., Liu, Q., Liu, J., 2023. Aeolian dust history since 14.4 cal. Ka BP ndicated by grain-size end members of Shayan loess in the southern Kazakhstan. Quat. Sci. 43, 46–56.
Sun, H., Song, Y., Chen, X., Cheng, L., Liu, H., 2020. Holocene dust deposition in the Ili Basin and its implications for climate variations in Westerlies-dominated Central Asia. Palaeogeog. Palaeoclimatol. Palaeoecol. 550, 109731.
Sun, Y., Wang, X., Liu, Q., Clemens, S.C., 2010. Impacts of post-depositional processes on rapid monsoon signals recorded by the last glacial loess deposits of northern China. Earth Planet. Sci. Lett. 289, 171–179.
Tang, Z., Mu, G., Chen, D., Wu, X., Ali, A., 2007. Eolian deposits in northern slope of Kunlun Mts and their palaeoenvironmental implications during the past 5000 years. Quat. Sci. 27, 598–606.
Teng, X., Zhang, Z., Han, W., Fang, Y., Ye, C., 2015. Grain-size Characteristics and Its Environmental Significance of Loess from Southern Tarim Basin. Acta Sediment. Sin. 33, 941–950.
Tian, S.C., Sun, J.M., Zhang, Z.L., Abdulov, S., Cao, M.M., Gadoev, M., Oimahmadov, I., 2021. Loess deposits in the Tajik Basin, Central Asia: chronology, provenance and palaeoclimatic implications since the Last Glacial. Boreas 50, 147–166.
Ujvari, G., Stevens, T., Molnar, M., Demeny, A., Lambert, F., Varga, G., Jull, A.J.T., Pall-Gergely, B., Buylaert, J.P., Kovacs, J., 2017. Coupled European and Greenland last glacial dust activity driven by North Atlantic climate. Proc. Natl. Acad. Sci. U. S. A. 114, E10632–E10638.
Vandenberghe, J., Renssen, H., van Huissteden, K., Nugteren, G., Konert, M., Lu, H.Y., Dodonov, A., Buylaert, J.P., 2006. Penetration of Atlantic westerly winds into Central and East Asia. Quat. Sci. Rev. 25, 2380–2389.
Wang, L., Jia, J., Li, G., Li, Z., Wang, X., Chen, F., 2018. Fine-grained quartz OSL dating chronology of loess sequence from southern Tajikistan: Implications for climate change in arid central Asia during MIS 2. J. Asian Earth Sci. 155, 116–123.
Wei, H., Wang, L., Azarmdel, H., Khormali, F., Frechen, M., Li, G., Chen, F., 2021. Quartz OSL dating of loess deposits since the late glacial in the Southeast of Caspian Sea. Quat. Int. 583, 39–47.
Yang, H., Li, G., Gou, S., Qian, J., Deng, Y., Zhang, Y., Jonell, T.N., Wang, Z., Jin, M., 2021. The close-space luminescence dated loess record from SW Junggar Basin indicates persistent aridity during the last glacial-interglacial cycle in lowlands of Central Asia. Palaeogeog. Palaeoclimatol. Palaeoecol. 584, 110664.
Yang, H., Li, G., Huang, X., Wang, X., Zhang, Y., Jonell, T.N., Jin, M., Chen, C., Zhao, W., Zhang, H., Wang, Z., Deng, Y., 2020a. Loess depositional dynamics and paleoclimatic changes in the Yili Basin, Central Asia, over the past 250 ka. Catena 195, 104881.
Yang, S.L., Li, D.X., Liu, N.N., Zan, J.B., Liu, W.M., Kang, J., Murodov, A., Fang, X.M., 2020b. Quartz optically stimulated luminescence dating of loess in Tajikistan and its paleoclimatic implications for arid Central Asia since the Lateglacial. Palaeogeog. Palaeoclimatol. Palaeoecol. 556, 109881.
Youn, J.H., Seong, Y.B., Choi, J.H., Abdrakhmatov, K., Ormukov, C., 2014. Loess deposits in the northern Kyrgyz Tien Shan: Implications for the paleoclimate reconstruction during the Late Quaternary. Catena 117, 81–93.
Zhang, J.R., Zhou, X.Y., Long, H., 2020. Late Quaternary loess accumulation at the Rudak section in Uzbekistan, central Asia: Chronology and palaeoclimate implications. Palaeogeog. Palaeoclimatol. Palaeoecol. 547, 109695.
Zan, J., Maher, Barbara, A., Yamazaki, T., Fang, X., Han, W., Kang, J., Hu, Z., 2023. Mid-Pleistocene links between Asian dust, Tibetan glaciers, and Pacific iron fertilization. Proc. Nat. Acad. Sci. U. S. A. 120 (24), e2304773120.
Zhang, Z., Zheng, Z., Meng, X., Lai, Z., Hou, Y., Ji, J., 2023. Gradually increasing precipitation since 20 ka as evidenced by loess dolomite abundance in the Ili Basin Central Asia. Catena 232, 107420.
Zhao, J., Liu, S., He, Y., Song, Y., 2009. Quaternary glacial chronology of the Ateaoyinake River Valley, Tianshan Mountains, China. Geomorphology 103, 276–284.
Zhao, S., Xia, D., Lü, K., 2022. Holocene aeolian dust accumulation rates across the Chinese Loess Plateau. Global Planet. Change 208, 103720.
Zhong, Y., Liu, Y., Yang, H., Yin, Q., Wilson, D.J., Lu, Z., Jaccard, S.L., Struve, T., Clift, P. D., Kaboth-Bahr, S., Larrasoana, J.C., Bahr, A., Gong, X., Zhao, D., Zhang, Y., Xia, W., Liu, Q., 2024. Orbital controls on north pacific dust flux during the late quaternary. Geophys. Res. Lett. 51, e2023GL106631.